THE JOURNAL OF PHYSICAL CHEMISTRY C
A JOURNAL OF THE AMERICAN CHEMICAL SOCIETY

pubs.acs.org/JPCC

Article

Evolution of the Magnetic and Structural Properties with the Chemical Composition in Oleate-Capped $Mn_xCo_{1-x}Fe_2O_4$ Nanoparticles

Marco Sanna Angotzi, Valentina Mameli,* Dominika Zákutná, Denisa Kubániová, Claudio Cara, and Carla Cannas

Cite This: *J. Phys. Chem. C* 2021, 125, 20626−20638

Read Online

ACCESS | Metrics & More | Article Recommendations | Supporting Information

ABSTRACT: Understanding the complex link among composition, microstructure, and magnetic properties paves the way to the rational design of well-defined magnetic materials. In this context, the evolution of the magnetic and structural properties in a series of oleate-capped manganese-substituted cobalt ferrites ($Mn_xCo_{1-x}Fe_2O_4$) with variable Co/Mn molar ratios is deeply discussed. Single-phase ferrites with similar crystallite and particle sizes (about 10 nm), size dispersity (14%), and weight percentage of capping oleate molecules (17%) were obtained by an oleate-based solvothermal approach. The similarities among the samples permitted the interpretation of the results exclusively on the basis of the actual composition, beyond the other parameters. The temperature and magnetic field dependences of the magnetization were studied together with the interparticle interactions by DC magnetometry. Characteristic temperatures (T_{max}, T_{diff}, and T_b), coercivity, anisotropy field, and reduced remanence were found to be affected by the Co/Mn ratio, mainly due to the magnetic anisotropy, interparticle interactions, and particle volume distribution. In addition, the cobalt and manganese distributions were hypothesized on the basis of the chemical composition, the inversion degree obtained by ^{57}Fe Mössbauer spectroscopy, the anisotropy constant, and the saturation magnetization.

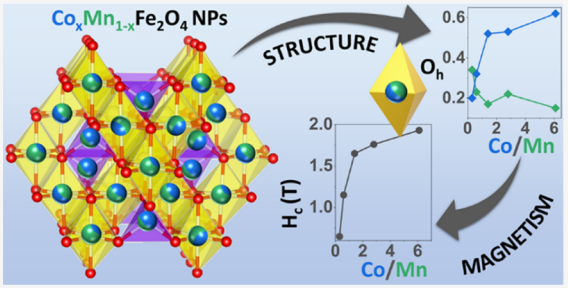

INTRODUCTION

Magnetic cubic ferrites with the formula MFe_2O_4 (where M stands for a divalent metal cation such as Fe^{II}, Co^{II}, Mn^{II}, etc.) crystallize in the spinel structure, which is described by a unit cell of 32 cubic close-packed oxide anions in which the metal cations occupy 8 tetrahedral (T_d-site) and 16 octahedral sites (O_h-site).[1,2] The stoichiometry, the nature of the divalent cations, and their distribution among these two types of interstitial sites (usually summed up by the so-called "inversion degree") are key features to modulate the magnetic properties (e.g., saturation magnetization and anisotropy) of the cubic ferrite, beyond size and shape changes.[1−3] Among these materials, cobalt ferrite ($CoFe_2O_4$) features the highest anisotropy constant (2.9×10^5 J m^{-3}),[2] which makes it the sole magnetically hard phase, but for some applications, the higher toxicity of cobalt ions in comparison with others has to be taken into account. Besides the size-,[4−6] shape-,[4,7−10] and coating-tuning[11−13] approaches, cation substitution (also improperly called doping) is a well-known strategy to modulate the properties of nanostructured spinels.[14−19] The co-presence of different types of divalent cations in the structure (i.e., the production of chemically mixed ferrites) represents a successful strategy to finely tune the magnetic behavior and reduce the toxicity of the final product.[1,2]

The magnetic properties of cobalt ferrite nanoparticles (NPs) have been modified by substituting cobalt ions with other divalent metals since the 2000s. In the beginning, attention was devoted to Co/Zn[20] or Co/Fe mixed ferrites.[21] Co/Mn chemically mixed ferrites were first proposed in 2009, in the form of spheroidal NPs or nanowires,[22,23] but the attention on these systems is still vivid with many recent studies published.[24−41] Indeed, manganese ferrite has 2 orders of magnitude lower anisotropy constant[2] but higher saturation magnetization[1] with respect to cobalt ferrite, and the co-presence of Co and Mn ions may lead to interesting physical and chemical properties exploitable for different applications, from magnetic stress sensoring[42] to catalysis.[43−46]

Many synthesis methods have been proposed for the synthesis of spinel ferrites with single or multiple divalent cations, from co-precipitation to solvothermal methods.[47] In particular, Co/Mn mixed ferrites have been synthesized by high-temperature thermal decomposition,[22] glycothermal process,[48−50] polyethylene glycol-assisted hydrothermal method,[51] polyol meth-

Received: July 12, 2021
Published: September 9, 2021

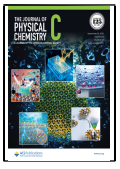

https://doi.org/10.1021/acs.jpcc.1c06211
J. Phys. Chem. C 2021, 125, 20626−20638

od,[52] mechanical milling,[28,53] co-precipitation method,[54−56] ceramic method,[57] and self-combustion.[58,59]

The complex system of relationships between the magnetic properties and other features of NPs, controllable by the chosen synthesis method (such as the chemical composition, particle size and size dispersity, cation distribution, spin canting, interparticle interactions, etc.), depict the difficulties in this research field in having a fully characterized set of samples with only one feature varying. Indeed, in the literature, few studies reported a discussion of the magnetic properties together with the chemical composition obtained by quantitative analytical methods, such as atomic absorption spectroscopy (AAS)[55] or inductively coupled plasma optical emission spectrometry (ICP−OES),[34] or semi-quantitative ones, such as scanning electron microscopy (SEM)−energy dispersive X-ray (EDX) analysis.[29,34,39,40,51,59] The crystallite size in the studied samples was found to change as a function of the Co/Mn ratio in the range of 14−22,[51] 16−34,[29] 23−33,[34,59] and 3.0−31.0 nm.[55] Some studies focused on a single intermediate chemical composition.[34,39,40] Most commonly, a study of the magnetic field[24,26,31,34,35,39,40,52,57,59−61] and/or temperature dependence[28,30,49,51,52,55,60,62] of the magnetization is reported, whereas only rarely an investigation of the interparticle interactions is provided.[28] In one case, the Co/Mn mixed ferrite NPs were used for comparison with bimagnetic core−shell NPs.[63]

Recently, our group has developed an oleate-based solvothermal method, which permitted us to prepare a wide variety of highly crystalline and homogeneously sized spinel ferrite-based nanosystems, from single phases[11,19] and chemical mixtures[64] to bi-magnetic core−shell[11,13,65] and optic-magnetic flower-like nanoarchitectures.[12]

In this work, the magnetic properties of the chemically mixed Co/Mn ferrite NPs prepared by the oleate-based solvothermal method with sizes around 10 nm[64] were studied by DC magnetometry based on their actual chemical composition, besides the influence of other structural or morphological parameters, that is, crystallite size, particle size, size dispersity, and organic capping content, that can be considered constant. The NP size at around 10 nm was chosen to obtain the smaller size dispersity with a single-step solvothermal synthesis, based on previous studies.[11,19] Temperature and magnetic field dependences of the magnetization and the role of the interparticle interactions are discussed, together with an estimation of the cation distribution of Co^{II} and Mn^{II} based on metal cation contents from ICP−OES and the Fe^{III} cation distribution from low-temperature in-field ^{57}Fe Mössbauer spectroscopy, anisotropy constants, and saturation magnetization values.

METHODS

Chemically mixed Co/Mn spinel ferrites were synthesized by the oleate-based solvothermal method reported elsewhere,[64] together with ICP−OES and X-ray diffraction (XRD) analyses.

The chemical composition was studied by ICP−OES. The dried samples were digested by using HNO_3 65% w/w. The digested sample solutions were stirred at room temperature for 1 h and then heated at 50 °C for 2 h. The solutions were left to cool, filtered, and diluted with distilled water to obtain a 2% w/w HNO_3 solution. The ICP measurements were performed on a Liberty 200 ICP Varian spectrometer under the following conditions: Fe line, 259.940 nm; Co line, 238.892 nm; Mn line, 257.610 nm; and Fe, Co, and Mn concentration range, 0.1−2 mg/L. The chemical formulas were calculated by assuming the absence of anion vacancies.

The weight percentage of capping oleate molecules was determined by ThermoGravimetric Analysis (TGA) by using a PerkinElmer STA 6000, in the 25-850 °C range, with a heating rate of 10 °C/min under 40 mL/min O_2 flow.

The samples were characterized using a PANalytical X'Pert PRO diffractometer equipped with a Cu anode ($\lambda_{K\alpha}$ = 1.5418 Å), a secondary monochromator, and a PIXcel position-sensitive detector. Calibration of the peak position and instrumental width was done by using powdered LaB_6 from NIST. The hexane dispersions were dried on a glass plate and measured in the angular range of 10−85° with a step of 0.039°. Refinement of the structural parameters was performed by the Rietveld method using MAUD software,[18] adopting the recommended fitting procedures.[66] Structural models of the identified phases were obtained by the Crystallographic Open Database (COD).

Transmission electron microscopy (TEM) micrographs were obtained by using a JEOL JEM 1400 PLUS operating at 120 kV. The particle size distribution was obtained by measuring in the automatic mode over 1000 particles through software Pebbles and adopting a spherical shape.[67] The mean particle diameter was calculated as the average value and the dispersity as the percentage ratio between the standard deviation and the average value.

DC magnetic properties were studied on powders with a Quantum Design PPMS DynaCool (H_{max} = 90 kOe) system by using the VSM module. Magnetization values were normalized for the amount of inorganic phase, based on thermogravimetric analyses. Different kinds of magnetic measurements were carried out. The field dependence of the magnetization (M vs H) was studied at 10 and 300 K between 70 and −70 kOe. The magnetic moment and domain size distributions were obtained by two different approaches (see the paragraph in the Supporting Information entitled "S4. Magnetic domain size and moment distribution by numerical inversion" for further details): a non-regularized inversion method using MINORIM software[68] and a regularized inversion method.[69,70] The input data were pre-treated by mathematical interpolation in the case of MINORIM method in order to get a 1000-point curve. For the second method, the raw data were used instead. The magnetic domain size (D_{MAG}) distribution from MINORIM software was estimated according to the following equation

$$(D_{MAG})_i = \sqrt[3]{\frac{6\mu_i a^3}{\mu_{uc}\pi}} \quad (1)$$

where a is the lattice parameter obtained by Rietveld refinement, μ_{uc} the magnetic moment of the unit cell of the spinel ferrite, and μ_i the ith magnetic moment value, calculated from M versus H recorded at 300 K. When using MINORIM for the calculation, a cut off of 1,500,000 A/m was considered for correcting the diamagnetic contribution; the minimum and maximum dipole moments were set as 1×10^{-22} and 1×10^{-17} A·m^2, respectively, and 36 bins were used for 6 subsets or optimized values for a Langevin dipole domain mode. The mean magnetic domain size $\langle D_{MAG}\rangle$ was then obtained as the value at the maximum in the M_s-weighted magnetic domain size (D_{MAG}) distribution obtained for the 36 bins and 6 subsets approach (which gave rise to a monomodal size distribution).

The saturation magnetization (M_s^{300K} and M_s^{10K}) was estimated by using the equation

https://doi.org/10.1021/acs.jpcc.1c06211
J. Phys. Chem. C 2021, 125, 20626−20638

Table 1. Experimental Composition Determined by ICP−OES; Cell Parameter (a), Crystallite Size (D_{XRD}), and Microstrain (ε) Determined by Rietveld Refinement on the XRD Patterns; Particle Size (D_{TEM}, V_{TEM}) and Related Standard Deviation (σ) of the Particle Size Distribution Obtained by TEM Analysis[a]

sample	Co/Mn ratio by ICP−OES	a (Å) by SPA	a (Å) by Rietveld	$\langle D_{XRD}\rangle$ (nm) by Rietveld - no ε	$\langle\langle D_{XRD}\rangle$ (nm) by Rietveld	$\langle\varepsilon\rangle$	$\langle D_{TEM}\rangle$ (nm)	$\sigma\langle D_{TEM}\rangle$ (%)	$\langle V_{TEM}\rangle$> (nm^3)	$\sigma\langle V_{TEM}\rangle$ (%)	% w/w of oleate molecules by TGA
Mn		8.48(1)	8.497(1)	9.5(1)	10.7(1)	0.004(1)	9.8	14	519	42	18(1)
Co23Mn77	0.3	8.46(1)	8.471(1)	9.6(1)	10.0(1)	0.002(1)	10.3	16	607	47	17(1)
Co37Mn63	0.6	8.44(1)	8.449(2)	9.5(1)	10.1(1)	0.003(1)	10.9	14	699	39	17(1)
Co59Mn41	1.4	8.42(1)	8.422(1)	9.0(1)	9.6(1)	0.003(1)	9.7	14	501	41	17(1)
Co74Mn26	2.8	8.40(1)	8.412(1)	9.2(1)	9.8(1)	0.003(1)	9.0	13	383	37	18(1)
Co86Mn14	6.1	8.40(1)	8.399(1)	10.4(1)	11.6(1)	0.004(1)	9.2	14	431	44	17(1)
Co		8.38(1)	8.393(1)	9.2(1)	10.3(1)	0.004(1)	9.1	14	427	48	16(1)
mean values[b]				9.5(5)	10.2(8)	0.0032(4)	9.7(8)	14.1(9)	$5(1)\times10^2$	43(4)	17(1)

[a]The XRD data were refined by using as a starting crystalline structure that of cobalt ferrite (#1533163 available on the COD). Weight percentage of capping oleate molecules obtained by TGA [b]Mean values calculated based on the values obtained for the Co/Mn mixed ferrite NPs.

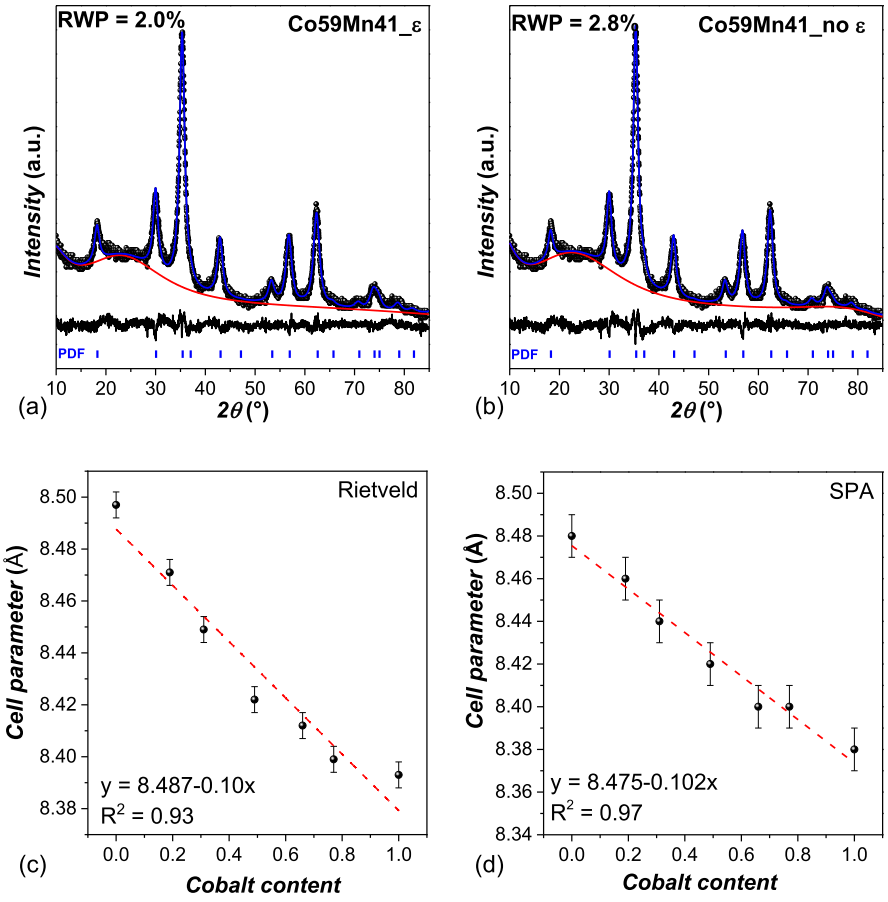

Figure 1. Rietveld refinement of the Co59Mn41 sample obtained with (a) and without microstrain (b). Trends of the lattice parameter calculated by Rietveld refinement (equal values were found for the two attempts carried out with and without microstrain) (c) or SPA (d) of the Co/Mn ferrite samples as a function of the actual cobalt content determined by ICP-OES. The red curve in (a,b) represents the amorphous contribution of the glass sample holder, while the red dashed line in (c,d) represents the linear curve fitting. The error bars in (c,d) represent the errors listed in Table 1 for a (Å) by Rietveld and a (Å) by SPA, respectively.

$$M = M_s\left(1 - \frac{a}{H} - \frac{b}{H^2}\right) \quad (2)$$

for H tending to ∞.[71] The temperature dependence of magnetization (M vs T) was studied by using the zero-field-cooled (ZFC) and field-cooled (FC) protocols: the sample was cooled down from 300 to 2 K in a zero magnetic field; then, the signals were recorded under a static magnetic field of 100 Oe. M_{ZFC} was measured during the warm-up from 2 to 300 K, whereas M_{FC} was recorded during the cooling step.

The anisotropy constant (K) was calculated as[72]

$$K = \frac{H_c M_s}{0.96\cdot\left(1 - \frac{T}{T_B}\right)^{0.77}} \quad (3)$$

https://doi.org/10.1021/acs.jpcc.1c06211
J. Phys. Chem. C 2021, 125, 20626−20638

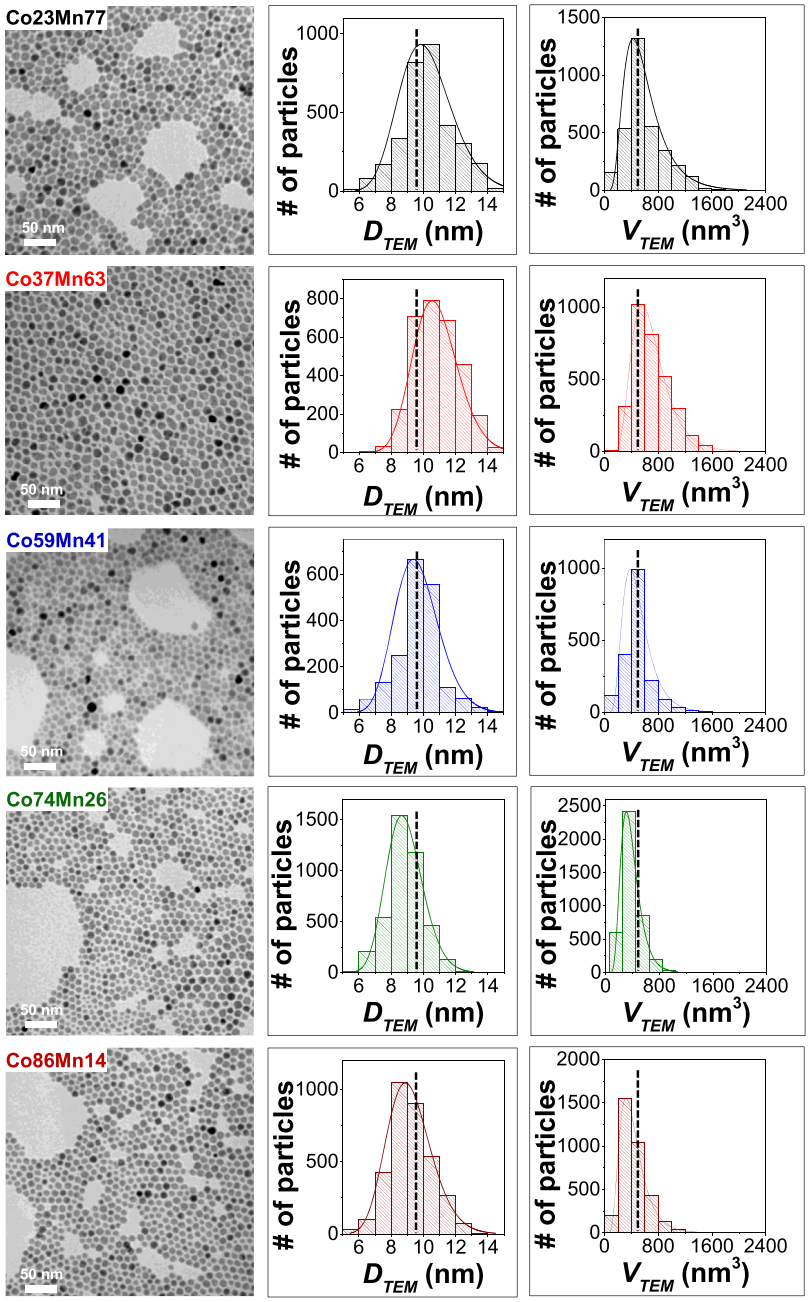

Figure 2. TEM bright-field micrographs of the samples and particle size distributions (as number (#) of particles per class of TEM-derived diameter, D_{TEM}, or volume, V_{TEM}). Solid lines on the histograms represent the curve fitting of the size distributions by the log-normal function. The dashed lines represent the mean values reported in Table 1 for D_{TEM} and V_{TEM}, calculated as the average of the values obtained for the Co/Mn ferrites samples.

Isothermal remanent magnetization (IRM) was measured according to the following steps: (i) demagnetization of the sample after cooling it in a zero magnetic field; (ii) setting a small field (of progressively higher intensity); (iii) switching off the magnetic field; and (iv) measurement of the remanence. For the direct current demagnetization (DCD) measurements, the same procedure was applied but starting from a negative saturated state (−70 kOe of the applied field).

ΔM was calculated according to Kelly's version of the Wohlfarth equation[73]

$$\Delta M = -m_{DCD}(H) - 1 + 2m_{IRM}(H) \quad (4)$$

where $m_{DCD}(H)$ and $m_{IRM}(H)$ are, respectively, the remanence values for the DCD and IRM curves divided for the maximum values at 70 kOe.

The acquisition of ^{57}Fe Mössbauer spectra was done in a transmission mode with the ^{57}Co source diffused into a Rh matrix, moving with a constant acceleration. The velocity calibration of the Wissel spectrometer was performed using a standard α−Fe foil, and the isomer shifts (ISs) are given relative to this standard at 296 K. For each sample, around 50 mg of powdered particles was encapsulated in an aluminum foil and measured in a helium bath cryostat from Janis Research at 4.2 K with an applied external magnetic field of 6 T perpendicular to the direction of the γ-beam. The fitting of the hyperfine parameters, using a standard least-squares fitting routine with

https://doi.org/10.1021/acs.jpcc.1c06211
J. Phys. Chem. C 2021, 125, 20626−20638

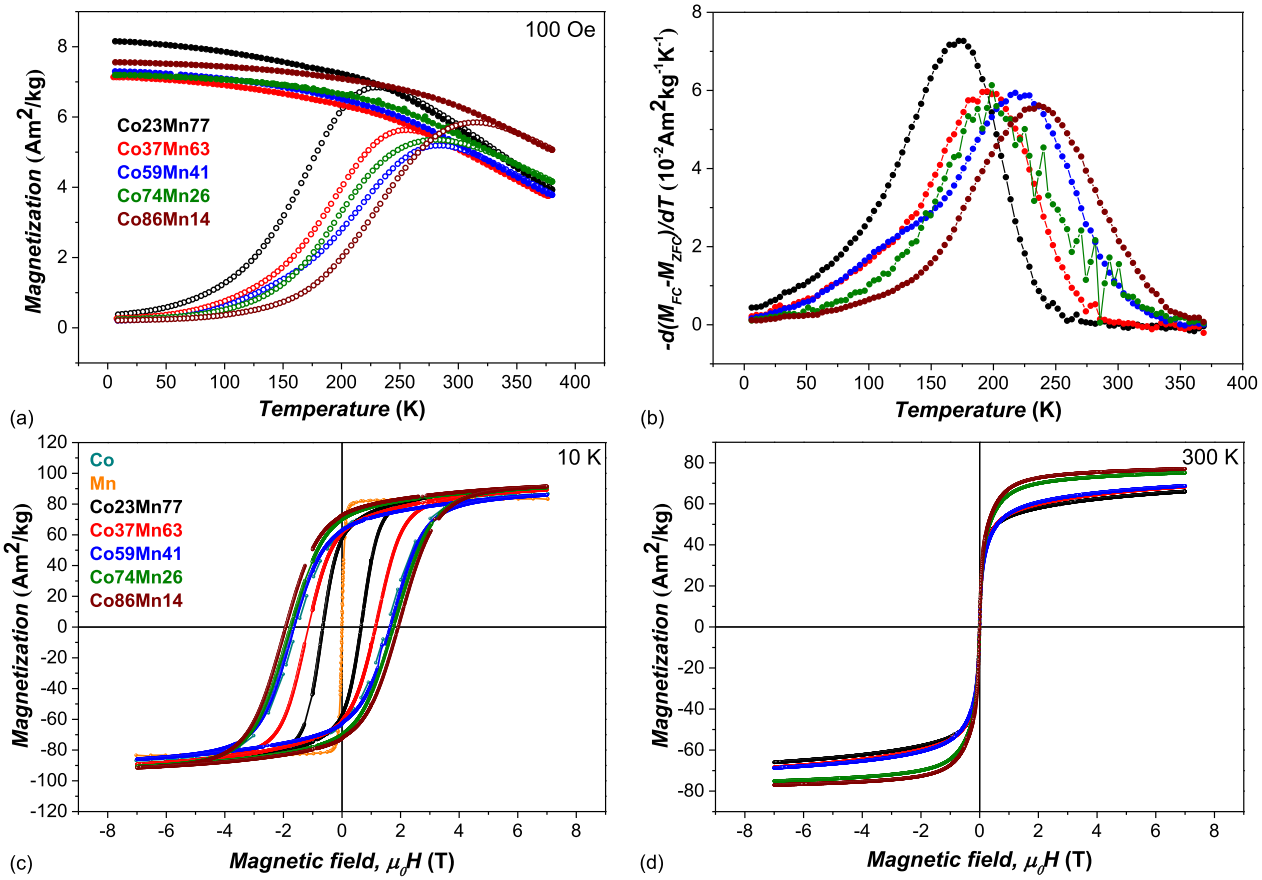

Figure 3. ZFC (empty circles) and FC (full circles) curves recorded at a low external magnetic field (10 mT) (a) and anisotropy energy barrier distributions estimated by the first derivative $-d(M_{FC}-M_{ZFC})/dT$ (b). Magnetization isotherms of the chemical mixtures recorded at 10 K (b) and 300 K (d). Magnetization values were normalized for the amount of inorganic phase, based on TGA.

Lorentzian spectral lines, was performed with SpectrRelax software.[74] A sextet component with the IS of 0.32(3) mm/s, quadrupole shift (QS) close to 0 mm/s, and hyperfine field B_{eff} of 6.2(2) T in the central part of Mössbauer spectra models the contribution of a paramagnetic Fe diluted in an aluminum foil originating from the experimental setup.

RESULTS AND DISCUSSION

Five samples of chemically mixed Co/Mn ferrite, cobalt ferrite, and manganese ferrite NPs were previously synthesized through an oleate-based solvothermal method.[64] The chemical composition of the oleate-capped ferrite NPs was determined for all samples by ICP−OES[64] for the inorganic counterpart and by TGA for the oleate molecule quantification. The results show (Table 1) the following: (i) stoichiometric cobalt ferrite (sample named Co, Co/Fe 1:2); (ii) a slight manganese deficiency in manganese ferrite (sample named Mn, Mn/Fe 0.8:2.1); (iii) Co/Mn mixed ferrite NPs with an almost constant iron content (2.09 ± 0.02) and a Co/Mn ratio of 6.1 and 0.3; and (iv) a 17% w/w of oleate capping for all samples.

The XRD patterns for all Co/Mn mixed ferrite samples were analyzed by the Rietveld method both with (Figures 1a and S1, right) and without microstrain contribution (Figures 1b and S1, left) by using as a starting crystalline structure that of cobalt ferrite ((#1533163) available on the COD). Indeed, attempts (not reported here), done by inserting Mn^{II} ions according to the ICP−OES estimated contents in the structure, did not lead to any significant difference in the results, probably due to the similarities among Mn^{II}, Co^{II}, and Fe^{III} in terms of X-ray interaction. The Rietveld analysis was also carried out for the extreme chemical compositions of the cobalt and manganese ferrite samples (Co and Mn samples) by using the corresponding structural files available in the COD (#1533163 and #2300585, respectively). The average crystallite sizes for the Co/Mn mixed ferrite samples were 10.2 ± 0.8 and 9.5 ± 0.5 nm, respectively, which are ∼1.5 nm larger than those obtained by the Scherrer equation (mean value of 8.5 ± 0.2 nm)[64] and without any trend as a function of the chemical composition (Table 1). These values are close to those of the reference cobalt and manganese ferrite samples (Table 1). The refinement done by adopting microstrain or no microstrain contribution did not lead to changes in the lattice parameter values, *a*, which decreased with increasing cobalt content for both Rietveld refinement and single-peak analysis (SPA) (Figure 1c,d, Table 1). The values found for the cobalt and manganese ferrites are in good agreement with those reported in the literature (8.3919 Å, PDF card: 022-1086 for cobalt ferrite and 8.4990 Å, PDF card: 010-0319 for manganese ferrite). The Co-dependent decrease in the lattice parameter was ascribed to the smaller ionic radius of Co^{II} (58 pm for T_d coordination, 74.5 pm for O_h high-spin coordination, and 65 pm for O_h low-spin coordination) compared to Mn^{II} (66 pm for T_d coordination, 83 pm for O_h high-spin coordination, and 67 pm for O_h low-spin coordination).[65,75]

https://doi.org/10.1021/acs.jpcc.1c06211
J. Phys. Chem. C 2021, 125, 20626−20638

Table 2. Basic Parameters Determined from the ZFC Curves and Magnetization Isotherms of Cobalt and Manganese Ferrite Chemical Mixtures[a]

sample	T_{max} (K)	T_{diff} (K)	T_b (K)	H_c^{10K} (T)	H_K^{10K} (T)	M_{7T}^{10K} ($Am^2 kg^{-1}$)	M_s^{10K} ($Am^2 kg^{-1}$)	M_r/M_s^{10K}	M_s^{300K} ($Am^2 kg^{-1}$)	$\langle D_{MAG}\rangle$ (nm)	K ($10^5 Jm^{-3}$)
Mn	79(2)	81(2)	18(1)	n.a.	n.a.	83(2)	86(3)	0.44(2)			
Co23Mn77	231(5)	235(5)	171(3)	0.65(1)	1.9(1)	91(3)	98(3)	0.59(2)	74(2)	7.1(5)	3.74(2)
Co37Mn63	259(5)	280(6)	194(4)	1.12(3)	3.0(1)	89(3)	98(3)	0.62(2)	77(2)	6.2(5)	6.37(3)
Co59Mn41	284(6)	303(6)	219(4)	1.65(1)	4.0(1)	86(3)	95(3)	0.65(2)	76(2)	5.6(5)	9.00(3)
Co74Mn26	282(6)	314(6)	197(4)	1.76(1)	4.3(1)	91(3)	98(3)	0.71(2)	79(2)	5.6(5)	9.99(4)
Co86Mn14	315(6)	328(7)	234(5)	1.92(1)	4.5(1)	91(3)	99(3)	0.74(2)	80(2)	5.7(5)	10.9(4)
Co	307(6)	336(7)	221(4)	1.53(1)	4.2(1)	87(3)	97(3)	0.65(2)			8.51(3)
Mix1:5	66(1)	299(6)	16(1)	n.a.	4.0(1)	79(2)	82(2)	0.11(1)			

[a] T_{max}, T_{diff}, and T_b correspond to the maximum, furcation point of the ZFC curve (2% of difference), and blocking temperature, respectively, the latter calculated as the maximum in the $-d(M_{FC}-M_{ZFC})/dT$ curve; H_c^{10K} and H_K^{10K} correspond to the coercivity and anisotropy field, respectively; M_{7T}^{10K}, M_s^{10K}, M_s^{300K}, M_r/M_s^{10K}, $\langle D_{MAG}\rangle$, and K are magnetization at 7 T, saturation magnetization values at 10 and 300 K, reduced remanence, magnetic domain size, and anisotropy constant, respectively. n.a. stands for not applicable. Magnetization values were normalized for the amount of inorganic phase, based on TGA.

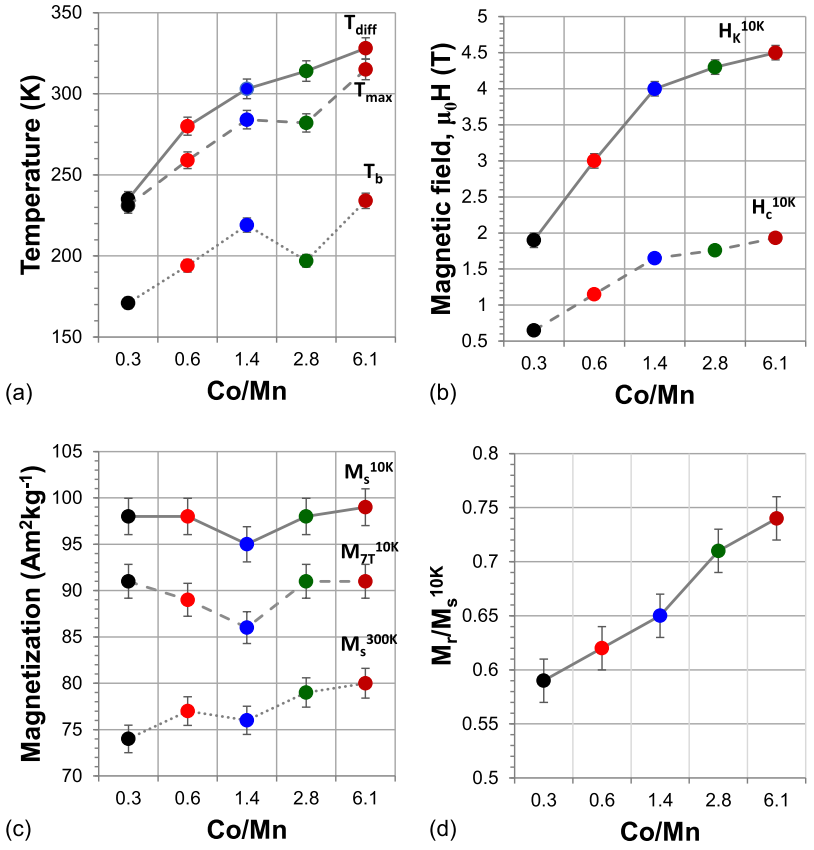

Figure 4. Trend of different magnetic parameters as a function of the Co/Mn ratio for the Co/Mn mixed ferrite samples. T_{max}, T_{diff}, and T_b correspond to the maximum, furcation point of the ZFC curve (2% of difference), and blocking temperature, respectively (a); H_c^{10K} and H_K^{10K} correspond to the coercivity and anisotropy field, respectively (b); M_{7T}^{10K}, M_s^{10K}, and M_s^{300K} represent the magnetization at 7 T and saturation magnetization values at 10 and 300 K, respectively (c); and M_r/M_s^{10K} indicates the reduced remanence (d).

A slightly better linear curve fitting (higher R^2 value) was obtained by SPA in comparison with the Rietveld method, but both led to similar intercept (≈8.48 Å) and slope (0.10) values.

Similar microstrain extent (quantified as two to five defects out of 10^4 lattice planes) was estimated for all samples (Table 1), in agreement with previous results on spinel ferrite-based NPs synthesized through similar synthetic approaches.[12,65]

TEM bright-field micrographs (Figures 2, S2) showed well-separated polygonal/spheroidal NPs for all samples with particle diameter (mean value of 9.7 ± 0.8 nm for the Co/Mn mixed ferrite samples) close to the crystallite size, unimodal diameter distributions, and mean dispersity for the Co/Mn mixed ferrite samples of 14.1 ± 0.9% (Table 1). Slight differences were observed between Co37Mn63 and Co23Mn77 samples, with higher manganese content with respect to the others. In particular, these samples exhibited slightly larger NPs ($\langle D_{TEM}\rangle$ equal to 10.9 and 10.3 nm, respectively). In addition, the Co59Mn41 sample, even though characterized by a monomodal D_{TEM} distribution, featured a second population of smaller NPs, as clearly visible in the TEM micrograph (Figure 2). To further deepen this aspect, particle volume distributions were also calculated (Figure 2), revealing log-normal distributions,

https://doi.org/10.1021/acs.jpcc.1c06211
J. Phys. Chem. C 2021, 125, 20626−20638

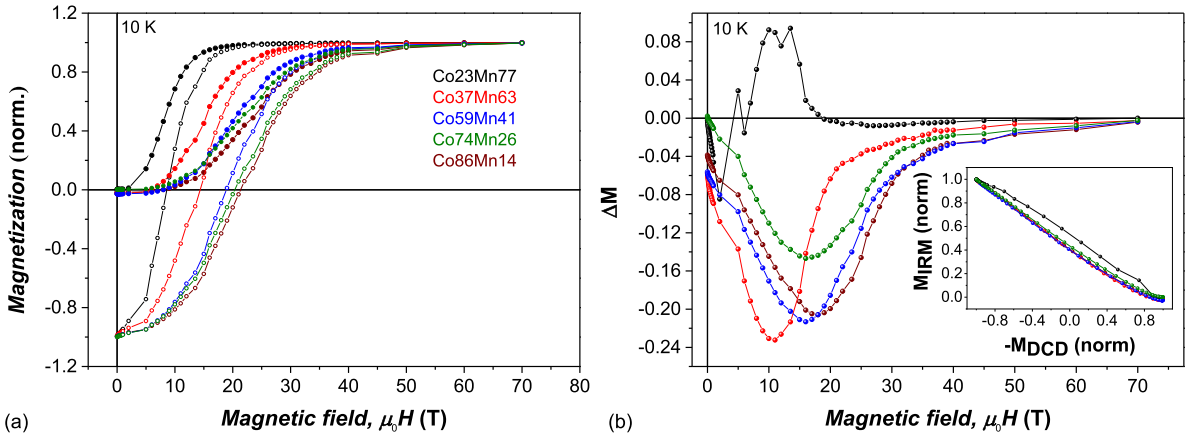

Figure 5. IRM (full circles) and DCD (empty circles) curves normalized between 0 and 1 and −1 and +1 (a), Δ*M* (b), and Henkel (inset) plots of the Co/Mn mixed ferrite samples.

broader in the case of Mn-rich samples, with the exception of Co59Mn41, whose distribution is characterized by a second population of smaller particles in addition to the principal one which is slightly shifted toward a higher mean volume value (Figure S3) if compared to the other Mn-rich samples.

As reported elsewhere,[18] a discussion of the magnetic properties of chemical mixtures as an exclusive function of the chemical composition can be carried out only if all the other structural and morphological parameters are kept constant since they have an influence on the magnetic properties. The set of samples described here served this purpose perfectly. Therefore, DC magnetometry measurements were carried out on all chemical mixtures (Figure 3, Table 2) and on the Co and Mn samples for comparison.

Both the temperature and magnetic field dependences of magnetization (*M* vs *T*, *M* vs *H*) showed a single-magnet behavior (i.e., a single peak in the *M* vs *T* curves obtained by ZFC−FC protocols and in the energy barrier distribution shown in Figure 3a,b; a single-stage loop in the *M* vs *H* curves at 10 K shown in Figure 3c) that, together with the actual chemical composition and changes in the lattice parameters, indicated the effectiveness of the synthesis method in producing chemically mixed ferrite NPs. For comparison with the Co/Mn mixed ferrites, a mechanical mixture of Co and Mn samples with a Co/Mn weight ratio equal to 1:5 was prepared and analyzed for its magnetic properties. The results, summarized in Table 2 and Figure S4, revealed a superposition of both the soft and hard magnetic behavior of the extreme ferrite compositions, a completely different behavior with respect to what was observed in the Co/Mn mixed ferrite samples.

The *M* versus *T* curves appeared similar for all samples with a general progressive shift of T_{max}, T_{diff}, and T_b toward lower temperatures with increasing manganese content (~80, 90, and 60 K of difference between the extreme Co/Mn mixed ferrite compositions, respectively), as expected for systems featuring progressively more soft magnetic behavior.[63] However, an odd behavior is found for the Co59Mn41 and Co74Mn26 samples (Figure 4a). Indeed, a lower T_b value for the Co74Mn26 and no differences in the T_{max} for Co59Mn41 and Co74Mn26 samples were found, even though the ZFC curves are differently shaped: those of the sample Co59Mn41 are a bit sharper but with a shoulder at a temperature lower than 200 K, which is also visible in the corresponding energy barrier distribution below 150 K. These findings are in agreement with the TEM analysis results (Figures 2, S3), which showed the presence of smaller NPs in addition to the main population in the Co59Mn41 sample.

In the *M* versus *H* curves at 10 K, a progressive decrease with manganese was also observed in the coercive field (H_c^{10K}) and anisotropy field (H_K^{10K}) (Figure 4b), with closer values for the Co-rich samples, which are also comparable with those of the cobalt ferrite sample (Co). The higher similarities among the Co-rich samples correspond to similar values of the mean magnetic diameter ($\langle D_{MAG} \rangle$, M_s-weighted by MINORIM with 36 bins and 6 subsets shown in Figures S5 and S6) and the anisotropy constant (K) (Table 2). A lowering of *K* with increasing manganese content was found, which reflects the lower single-ion anisotropy constant of Mn^{II} with respect to Co^{II},[63,76] as already observed by the previous characterization through room-temperature ^{57}Fe Mössbauer spectroscopy.[64] $\langle D_{MAG} \rangle$ was found to be higher for the Mn-rich samples, in agreement with the slightly higher $\langle D_{TEM} \rangle$ values. If the number-weighted magnetic domain size distributions are calculated for the samples and compared with the D_{TEM} distributions (Figure S7, see the paragraph on the Supporting Information entitled "S4. Magnetic domain size and moment distribution by numerical inversion" for further details), it is possible to highlight for all samples a shift of the magnetic domain size distribution toward lower values, probably due to spin structure inhomogeneities. Depending on how the magnetic domain size distribution is calculated (Figures S5, S6, and S8), the second population of smaller particles observed for the sample Co59Mn41 is reflected in the distribution of the magnetic moment and magnetic domain size. Considering these trends, the lowering of magnetic anisotropy seemed to be the most crucial parameter in defining the shift toward lower values of the characteristic temperatures in the *M* versus *T* curves. The magnetization at 7 T and the saturation magnetization at 10 K were about 90 and 100 Am^2/kg, respectively, for all Co-containing samples, with no remarkable differences, while for the Mn sample, slightly lower values were obtained (83 and 86 Am^2/kg, Table 2, Figure 4c). Also, at 300 K, similar saturation magnetization values are found for all Co/Mn mixed ferrite samples (about 77 Am^2/kg) with a superparamagnetic behavior and slightly higher magnetization values along the whole curve for the Co74Mn26 and Co86Mn14 samples (Figure 3d). The reduced remanence at 10 K (M_r/M_s^{10K}, Table 2 and Figure 4d) was found in the range 0.59−0.74, due to a mixed cubic/uniaxial

https://doi.org/10.1021/acs.jpcc.1c06211
J. Phys. Chem. C 2021, 125, 20626−20638

anisotropy[18] with a progressive shift toward cubic anisotropy (the theoretical value is 0.83)[77] as the Co content increases.

The observed saturation magnetization values appeared higher than those usually observed in the literature for Co/Mn mixed ferrite NPs[29,30,39,40,51,55,56,59,61,78,79] from about 30 to 70 Am^2/kg, due to differences in the particle size and particle size distribution, the presence of dead layers of canted surface spins, and cation distribution. However, the values are close to those observed for other spinel ferrite systems produced by the same oleate-based solvothermal method.[13]

To deeply study the role of interactions in the magnetic behavior of the samples, DCD and IRM protocols were adopted at 10 K (Figure 5a). The IRM and DCD curves appeared similar for the Co-rich samples, in particular, for Co86Mn14 and Co74Mn26, whereas those of the Co23Mn77 and Co37Mn63 samples are quite different, reaching saturation at lower fields in comparison with the Co-rich samples (about 20 and 30 kOe for Co23Mn77 and Co37Mn63, respectively, against about 50 kOe for the others). Figure 5b and its inset show the ΔM plot[73] and the Henkel plot,[80] respectively. Both these graphs provided evidence of deviations in the samples' behavior with respect to the ideal case of non-interacting single-domain NPs. In particular, negative values of ΔM or the upward concave curve in the Henkel plot are considered to be caused by demagnetizing dipolar interactions or also by an inhomogeneous spin structure,[81] while positive ΔM and the downward concave curve in the Henkel plot are due to magnetizing interactions, for instance, exchange interactions,[82,83] or can be caused by cubic anisotropy.[83] The results indicated the predominance of weak dipolar interactions and/or a more inhomogeneous spin structure for all samples but Co23Mn77, which seemed to be characterized by weak exchange interactions or cubic anisotropy NPs. The positive ΔM peak found for this sample is actually much lower in its intensity (about 0.08) with respect to the ΔM negative peaks of the other samples (about 0.14−0.23), suggesting even weaker interactions. Nevertheless, the different behavior observed for this sample might suggest a certain degree of contact between the surface atoms of the NPs, that is, a certain degree of agglomeration and a less homogeneous oleate capping. However, these reasons can be excluded based on TEM and TGA data, respectively. A second explanation concerns cubic anisotropy, but the discussion appears more complex. Indeed, M_r/M_s values for all samples are found between 0.6 and 0.74, suggesting the coexistence of cubic and uniaxial anisotropy to a similar extent.[18] Therefore, one might conclude that if cubic anisotropy is responsible for the positive ΔM peak in Co23Mn77, in the other samples this contribution is masked by stronger dipolar interactions or a more inhomogeneous spin structure, which seems to follow the anisotropy constant trend. Indeed, it is worth mentioning that K of Co37Mn63 is almost 1.8 times that of the Co23Mn77 one. The position of the ΔM negative peaks increased toward a higher magnetic field in the order of Co37Mn63 $\ll$ Co59Mn41 $\approx$ Co74Mn26 $<$ Co86Mn14, which is again coherent with an increase in the magnetic anisotropy (see the K values in Table 2), due to increasing cobalt ion content. The shapes of the ΔM negative peaks for these samples in terms of intensity and broadness were also different: (i) the Co37Mn63 sample was characterized by a sharper and more intense peak; (ii) the Co59Mn41 and Co86Mn14 samples exhibited very similar curves (although the second one is slightly shifted towards higher field values); and (iii) a broad and weaker peak was visible for the Co74Mn26. These results help shed light on the differences/similarities found in the ZFC−FC curves of the samples, which are affected by the particle volume, magnetic anisotropy, and magnetic interparticle interactions. In particular, the sample Co37Mn63 featured lower T_{max} (T_{diff} and T_b) with respect to the Co-rich samples due to lower magnetic anisotropy and weaker dipolar interactions. In the Co59Mn41 and Co74Mn26 samples, the difference in the cobalt content was probably compensated by lower dipolar interactions in the latter sample (weaker ΔM peak) together with slightly smaller NPs as revealed by the TEM analysis, leading to almost equal T_{max} values and lower T_b for the Co74Mn26 sample.

The first derivative of the DCD and IRM curves associated with the irreversible susceptibility gave similar distributions centered at the same magnetic field values for the DCD−IRM pairs for each sample (Figure S10) but shifted in agreement with an increase in the cobalt content. The absence of any shift in the DCD derivative distributions with respect to the IRM counterparts, expected in the case of dipolar interactions, may suggest that the most relevant contribution to the negative peaks observed in the ΔM plots is due to inhomogeneities in the spin structure. In addition, an increase in the broadness of the curves is observed as a function of the Co content, and with great similarities among those of the Co-rich samples. These findings agreed with the results obtained by other authors that provided, to the best of our knowledge, the only available paper in the literature about the study of the magnetic interactions in Co/Mn mixed ferrites.[28] In that work, the cobalt substitution degree in about 10 nm-sized particles produced remarkable differences in the magnetic properties in terms of magnetic anisotropy, coercivity, and interparticle interactions. All samples were found to feature dipolar interactions, with a direct correlation between the intensity of interactions and single-particle anisotropy.

In a previous publication, room-temperature ^{57}Fe Mössbauer spectra of the samples were recorded, revealing the absence of Fe^{II} and cubic symmetry from the IS and QS values, respectively. A decrease in the hyperfine field (B_{hf}) values with increasing Mn content for both octahedral and tetrahedral sites was observed, with a stronger effect for the latter one due to the preference of Mn ions for the four-fold coordination.[64] In this work, in order to determine the cationic distribution of iron ions in the spinel structure, in-field low-temperature ^{57}Fe Mössbauer spectra were recorded for all samples (Figure 6a), thus enabling the separation of overlapping spectral components which model the contribution of ^{57}Fe nuclei in tetrahedral and octahedral sites.

Since the Co/Mn mixed ferrites NPs at a liquid helium temperature are in a blocked state, two well resolved sextets associated with the Fe^{III} ions located in tetrahedral and octahedral sites of the ferrimagnetic spinel ferrite could be clearly discerned for all samples. Considering the fact that the presence of Co^{II} and Mn^{II} ions in the sites nearest to the resonating ^{57}Fe nuclei manifests itself in a broadening of the spectral lines, each sextet was modeled by a convolution of Lorentz lines (full width at half-maximum $\sim$ 0.29 mm/s) with a distribution of hyperfine fields (see curves in Figure 6b). The strong correlation of fit parameters did not allow us to unambiguously resolve the individual distributions of hyperfine fields. However, regardless of the choice of physically reasonable cut-off of effective hyperfine fields, every fit provided the same area fraction of the given component (i.e., the relative occupancies) and hyperfine parameters within the experimental

https://doi.org/10.1021/acs.jpcc.1c06211
J. Phys. Chem. C 2021, 125, 20626−20638

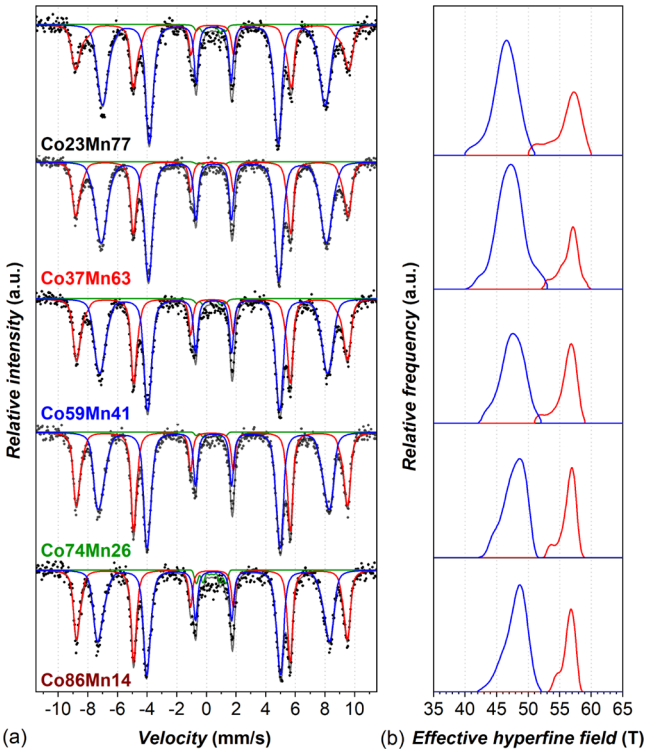

Figure 6. ^{57}Fe Mössbauer spectra (a) of the Co/Mn mixed ferrite samples in an applied field of B_{ext} = 6 T at liquid helium temperature (4.2 K) fitted by two sextets with a distribution of hyperfine fields (b) that represent Fe^{III} in the tetrahedral sublattice (red curve), that is, (Fe^{III}) and Fe^{III} in the octahedral sublattice (blue curve), that is, [Fe^{III}]. The minor sextet (green component) with the IS = 0.32(3) mm/s, QS close to 0 mm/s, and hyperfine field B_{eff} = 6.2(2) T represents a parasitic signal originating from the experimental setup.

error. The hyperfine parameters determined from ^{57}Fe Mössbauer spectra are listed in Table 3.

The obtained IS (0.38 ± 0.02 and 0.49 ± 0.02 mm/s for T_d and O_h, respectively) and QS values close to zero are those typical for spinel ferrites.[18] The mean effective field ($\overline{B_{eff}}$) appears almost constant for Fe^{III} ions in the tetrahedral sites, whereas that for octahedrally coordinated ions increases (of about 0.5 T) with the cobalt content until a plateau is reached for the two Co-richest samples (Co74Mn26 and Co86Mn14), as already observed for the room temperature measurements.[64] Indeed, also in this case, the data can be fitted by the CME model (Figure 7), obtaining a R^2 factor of 0.97 and a saturation

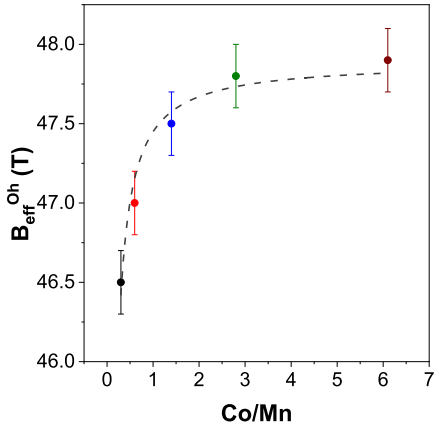

Figure 7. Evolution of mean effective field ($\overline{B_{eff}}$) in octahedral (O_h) sites as a function of the Co/Mn ratio for the Co/Mn mixed samples.

hyperfine field equal to 47.9 T, indicating a strong dependence of the hyperfine field in octahedral sites on the anisotropy constant. In addition, a change in the distribution of hyperfine fields for both interstitial sites was visible, due to different local environments of ^{57}Fe nuclei in agreement with the different chemical composition. In particular, with increasing Mn content, more symmetric distributions are obtained for octahedral sites, while those for tetrahedral sites become broader toward lower values. This indicates again a preference of Mn cations for tetrahedral coordination, in agreement with the room temperature study.[64]

The mean angle between the γ-beam and the vector B_{eff}, θm, might be related to the mean size of particles within the framework of a core−shell model, which assumes randomly oriented magnetic moments in the surface layer, that is, the shell and well-ordered magnetic moments in the core of the NPs.[84,85] Due to the enhanced anisotropy at the surface, not even the external magnetic field as high as 6 T is sufficient to align all magnetic moments in the shell to the direction of the applied field, observed as the deviation of the ratio of spectral line intensities $b = I_{2,5}/I_{3,4} = 4 \sin(2\theta m)/(1 + \cos(2\theta m))$, where I_i is

Table 3. Hyperfine Parameters Determined from the Mössbauer Spectra of the Samples Recorded at a Low Temperature (4.2 K) in the External Magnetic Field of 6 T: Values of the IS, QS, Mean Effective Hyperfine Field at 6 T (B_{eff}), Area Fraction of the Given Component (A), Ratio of Line Intensities $I_{2,5}/I_{3,4}$ (b), Mean Angle between the γ-Beam and the Vector B_{eff} (θm), and Chemical Formula Calculated from Site Occupancy Corrected by ICP−OES Data

sample	site	IS (mm/s)	QS (mm/s)	$\overline{B_{eff}}$ (T)	A (%)	b	θm (deg)	cation distributions
Co23Mn77	T_d	0.39(3)	−0.02(3)	56.2(3)	34.7(9)	3.1(1)	69.3(7)	$(M^{II})_{0.25}(Fe^{III})_{0.73}[M^{II}]_{0.59}[Fe^{III}]_{1.38}O_4$
	O_h	0.49(2)	0.01(3)	46.3(3)	65.3(9)			
Co37Mn63	T_d	0.37(2)	−0.01(2)	56.5(2)	33.3(6)	3.22(8)	70.8(4)	$(M^{II})_{0.28}(Fe^{III})_{0.70}[M^{II}]_{0.55}[Fe^{III}]_{1.41}O_4$
	O_h	0.49(2)	0.01(2)	47.1(2)	66.7(6)			
Co59Mn41	T_d	0.37(2)	0.00(3)	56.1(3)	39.3(7)	3.17(9)	70.1(5)	$(M^{II})_{0.16}(Fe^{III})_{0.83}[M^{II}]_{0.67}[Fe^{III}]_{1.28}O_4$
	O_h	0.49(2)	0.01(3)	47.5(3)	60.7(7)			
Co74Mn26	T_d	0.37(3)	0.00(3)	56.3(2)	41.2(6)	3.22(9)	70.8(6)	$(M^{II})_{0.14}(Fe^{III})_{0.85}[M^{II}]_{0.76}[Fe^{III}]_{1.22}O_4$
	O_h	0.48(2)	0.01(3)	47.8(3)	58.8(6)			
Co86Mn14	T_d	0.37(2)	0.00(2)	56.4(2)	41.2(6)	3.0(1)	68.3(7)	$(M^{II})_{0.14}(Fe^{III})_{0.85}[M^{II}]_{0.76}[Fe^{III}]_{1.22}O_4$
	O_h	0.48(3)	0.00(2)	48.0(3)	58.8(6)			

https://doi.org/10.1021/acs.jpcc.1c06211
J. Phys. Chem. C 2021, 125, 20626−20638

the intensity of the ith spectral line, from its limit values (4 for completely aligned magnetic moments along the direction of the applied magnetic field and 2 for disordered magnetic moments).[86,87] The narrow variance of θm values provided in Table 3 around ∼70° is in excellent agreement with the similarity in the mean sizes of NPs within the sequence of studied samples determined by both XRD and TEM.

Assuming the same *f*-factors for the individual spectral components and no vacancies, the relative fraction of iron ions within the two coordination types, together with the chemical composition obtained by ICP−OES,[64] indicates that, as the structure accommodates more cobalt ions, the iron ions move to the tetrahedral sites, revealing three values of inversion degree (γ): ∼0.57 for the samples with the highest manganese content (Co23Mn77 and Co37Mn63), 0.67 for the sample with an intermediate composition (Co59Mn41), and 0.76 for the samples with the highest cobalt content (Co74Mn26 and Co86Mn14). These results agree with the general tendency observed in manganese and cobalt ferrite, both in bulk (γ = 0.2 and γ = 1, respectively)[88] and in nanostructured (γ = 0.5[11,19,64,89] and γ = 0.7,[18,90−92] respectively) single M^{II} ferrites. Notably, the two Co-richest samples exhibited exactly the same iron cation distribution, in agreement with many similarities in the magnetic properties.

On the basis of the Co, Mn, and Fe contents from ICP−OES, the iron ion distribution obtained by ^{57}Fe Mössbauer spectroscopy, the saturation magnetization, and the anisotropy constant values, attempts to define the cation distribution of Co^{II} and Mn^{II} for the different samples were made according to the Néel model, which accounts for the existence of two magnetic sublattices in cubic ferrites.[18] The best results obtained are reported in Table S1. First, the cobalt distribution was estimated based on the trend of the magnetic anisotropy, which is mainly affected by the single-ion anisotropy of cobalt ions in the tetrahedral (-7.9×10^{-23} J/ion) and octahedral (8.5×10^{-22} J/ion) sites. The theoretical set of values are found compatible with the experimental trends (Tables S2,S3,S4) if all the cobalt ions (up to about 0.50 per formula unit) are located in the octahedral sites, coherent with the preference of cobalt ions for this kind of coordination. Only for the samples Co74Mn26 and Co86Mn14, it is necessary to hypothesize a small fraction of cobalt in the tetrahedral sites (0.12 and 0.16 per formula unit). Based on this hypothesis, the manganese distribution was estimated in order to obtain a theoretical saturation magnetization compatible with the experimental values. In this case, for the samples with the highest manganese content (Co23Mn77, Co37Mn63, and Co59Mn41), a good agreement (Tables S2−S4) between experimental and theoretical values is obtained with about a 50:50 manganese ions in the octahedral and tetrahedral sites in agreement with the value of inversion degree generally found for manganese ferrite NPs (γ = 0.50). It is worth noting that a certain deviation is obtained in particular for the Co23Mn77 and Co37Mn63 samples concerning the total amount of octahedrally coordinated metal cations per formula unit (Table S3), which made us to consider the presence of a small percentage of vacancies in the octahedral sites (0.08−0.05 per formula unit, respectively). This is necessary in order to lower the obtained saturation magnetization to reasonable values (about 100 Am^2/kg) closer to the experimental ones (98 Am^2/kg) (Table S4). However, the discrepancy between theoretical and experimental low-temperature M_s is somehow expected since it is also observed for bulk manganese ferrite (theoretical and experimental magnetic moments per molecule equal to 5 and 4.6 μ_B, respectively) and cobalt ferrite (3 and 3.7 μ_B, respectively). These deviations from theory are usually ascribed to the non-quenched orbital moments and the spinel structure.[1]

CONCLUSIONS

Mixed Co/Mn ferrites having variable Co/Mn molar ratios (6.1, 2.8, 1.4, 0.6, and 0.3) were prepared by an oleate-based solvothermal approach and studied for their magnetic behavior. With the sample being similar in the iron content (2.09 ± 0.02) per formula unit, crystallite and particle sizes (about 10 nm), size dispersity (14%), and weight percentage of capping oleate molecules (17%), the magnetic properties were discussed exclusively on the basis of Co/Mn ratio. Similar and high saturation magnetization at 10 and 300 K were found due to different chemical compositions and cation distributions, as hypothesized by the Néel sub-lattices model. In general, magnetic anisotropy was found to be the key parameter affecting the trend in other magnetic parameters (T_{max}, T_{diff}, T_b, H_c, H_K, and M_r/M_s) due to the different cobalt content with some exceptions associated with a complex interplay between anisotropy, interparticle interactions, and details in the particle volume distribution. In particular, deviations from the ideal case of non-interacting NPs were found by IRM-DCD protocols for all samples, with dipolar interactions as predominant (negative ΔM peak) and with a correlation between cobalt content and magnetic anisotropy. Only the sample with the lowest cobalt content exhibited a positive ΔM peak, which probably accounts for the unmasked cubic anisotropy as a result of weaker dipolar interactions. Moreover, in an attempt to define the cation distribution based on Co, Mn, and Fe contents from ICP−OES, the iron ion distribution obtained by ^{57}Fe Mössbauer spectroscopy, the saturation magnetization, and anisotropy constant values revealed some general trends in the crystalline structure of these chemically mixed spinel ferrites as a function of the composition. In particular, the samples can be distinguished into two groups: (i) those with manganese content up to about 40% of total divalent cations characterized by Mn^{II} ions equally distributed in the two types of interstitial sites and Co^{II} present only in the octahedral sites and (ii) Co-richer samples having all the Mn^{II} cations in the octahedral sites.

ASSOCIATED CONTENT

Supporting Information

The Supporting Information is available free of charge at https://pubs.acs.org/doi/10.1021/acs.jpcc.1c06211.

Rietveld refinements on XRD patterns; TEM micrographs and particle size distribution of cobalt and manganese ferrite NPs; TEM particle volume distributions; ZFC−FC curves and magnetization isotherms at 10 K for cobalt and manganese ferrite NPs and their mixture; magnetic domain size and moment distribution by numerical inversion; first derivative of IRM and DCD curves; and theoretical cation distribution and spinel ferrite stoichiometry (PDF)

AUTHOR INFORMATION

Corresponding Author

Valentina Mameli − *Department of Chemical and Geological Sciences, University of Cagliari, 09042 Monserrato, Italy; Consorzio Interuniversitario Nazionale per La Scienza e Tecnologia Dei Materiali (INSTM), 50121 Firenze, Italy;*

https://doi.org/10.1021/acs.jpcc.1c06211
J. Phys. Chem. C 2021, 125, 20626−20638

orcid.org/0000-0002-1899-8636;
Email: valentina.mameli@unica.it

Authors

Marco Sanna Angotzi − *Department of Chemical and Geological Sciences, University of Cagliari, 09042 Monserrato, Italy; Consorzio Interuniversitario Nazionale per La Scienza e Tecnologia Dei Materiali (INSTM), 50121 Firenze, Italy;* orcid.org/0000-0003-1593-5872

Dominika Zákutná − *Department of Inorganic Chemistry, Charles University, 128 40 Prague 2, Czech Republic;* orcid.org/0000-0001-9417-6514

Denisa Kubániová − *Department of Low Temperature Physics, Faculty of Mathematics and Physics, Charles University, 180 00 Prague, Czech Republic*

Claudio Cara − *Department of Chemical and Geological Sciences, University of Cagliari, 09042 Monserrato, Italy; Consorzio Interuniversitario Nazionale per La Scienza e Tecnologia Dei Materiali (INSTM), 50121 Firenze, Italy*

Carla Cannas − *Department of Chemical and Geological Sciences, University of Cagliari, 09042 Monserrato, Italy; Consorzio Interuniversitario Nazionale per La Scienza e Tecnologia Dei Materiali (INSTM), 50121 Firenze, Italy;* orcid.org/0000-0003-2908-7739

Complete contact information is available at: https://pubs.acs.org/10.1021/acs.jpcc.1c06211

Notes

The authors declare no competing financial interest.

■ ACKNOWLEDGMENTS

The authors are much obliged to Prof. Daniel Niznanský from the Charles University of Prague for his invaluable scientific contribution to ^{57}Fe Mössbauer spectroscopy and fruitful discussions. PON AIM (PON Ricerca e Innovazione 2014−2020-Azione I.2-D.D. n.407 del 27 febbraio 2018 "Attraction and International Mobility", Cult-GeoChim project n. AIM1890410-3) is gratefully acknowledged for financing the fixed-term researcher fellowship of V. Mameli. CESA Project—RAS Piano Sulcis and Fluorsid S.p.A. are gratefully acknowledged for financing the post-doctoral fellowship of M. Sanna Angotzi and C. Cara, respectively. Thanks are due to Centro Servizi di Ateneo per la Ricerca (CeSAR) for the use of the PPMS DynaCool facility for the DC magnetometry measurements and for the TEM measurements performed with the JEOL JEM 1400 PLUS. This work was supported by the Fondazione di Sardegna, Italy, Fondazione di Sardegna (FdS) Project: CUP F72F20000240007(2019): "Surface-tailored Materials for Sustainable Environmental Applications". This work was also supported by Czech Science Foundation (grant number 19-02584S) and by Charles University Research Centre program no. UNCE/SCI/014.

■ REFERENCES

(1) Cullity, B. D.; Graham, C. D. *Introduction to Magnetic Materials*; Wiley, 2009.
(2) Coey, J. M. D. *Magnetism and Magnetic Materials*; Cambridge University Press: New York, 2010.
(3) West, A. R. *Solid State Chemistry and Its Applications*; Wiley, 2005.
(4) Jana, N. R.; Chen, Y.; Peng, X. Size- and Shape-Controlled Magnetic (Cr, Mn, Fe, Co, Ni) Oxide Nanocrystals via a Simple and General Approach. *Chem. Mater.* **2004**, *16*, 3931−3935.
(5) Zákutná, D.; Vlček, J.; Fitl, P.; Nemkovski, K.; Honecker, D.; Nižňanský, D.; Disch, S. Noncollinear Magnetism in Nanosized Cobalt Chromite. *Phys. Rev. B* **2018**, *98*, 064407.
(6) Zákutná, D.; Alemayehu, A.; Vlček, J.; Nemkovski, K.; Grams, C. P.; Nižňanský, D.; Honecker, D.; Disch, S. Critical Size Limits for Collinear and Spin-Spiral Magnetism in $CoCr_2O_4$. *Phys. Rev. B* **2019**, *100*, 184427.
(7) Zeng, H.; Rice, P. M.; Wang, S. X.; Sun, S. Shape-Controlled Synthesis and Shape-Induced Texture of $MnFe_2O_4$ Nanoparticles. *J. Am. Chem. Soc.* **2004**, *126*, 11458−11459.
(8) Xie, J.; Yan, C.; Zhang, Y.; Gu, N. Shape Evolution of "Multibranched" Mn-Zn Ferrite Nanostructures with High Performance: A Transformation of Nanocrystals into Nanoclusters. *Chem. Mater.* **2013**, *25*, 3702−3709.
(9) Cheon, J.; Kang, N.-J.; Lee, S.-M.; Lee, J.-H.; Yoon, J.-H.; Oh, S. J. Shape Evolution of Single-Crystalline Iron Oxide Nanocrystals. *J. Am. Chem. Soc.* **2004**, *126*, 1950−1951.
(10) Sathya, A.; Guardia, P.; Brescia, R.; Silvestri, N.; Pugliese, G.; Nitti, S.; Manna, L.; Pellegrino, T. $Co_xFe_{3-x}O_4$ Nanocubes for Theranostic Applications: Effect of Cobalt Content and Particle Size. *Chem. Mater.* **2016**, *28*, 1769−1780.
(11) Sanna Angotzi, M.; Musinu, A.; Mameli, V.; Ardu, A.; Cara, C.; Niznansky, D.; Xin, H. L.; Cannas, C. Spinel Ferrite Core-Shell Nanostructures by a Versatile Solvothermal Seed-Mediated Growth Approach and Study of Their Nanointerfaces. *ACS Nano* **2017**, *11*, 7889−7900.
(12) Sanna Angotzi, M.; Mameli, V.; Cara, C.; Grillo, V.; Enzo, S.; Musinu, A.; Cannas, C. Defect-Assisted Synthesis of Magneto-Plasmonic Silver-Spinel Ferrite Heterostructures in a Flower-like Architecture. *Sci. Rep.* **2020**, *10*, 17015.
(13) Sanna Angotzi, M.; Mameli, V.; Cara, C.; Musinu, A.; Sangregorio, C.; Niznansky, D.; Xin, H. L.; Vejpravova, J.; Cannas, C. Coupled hard-soft spinel ferrite-based core-shell nanoarchitectures: magnetic properties and heating abilities. *Nanoscale Adv.* **2020**, *2*, 3191−3201.
(14) Masrour, R.; Hamedoun, M.; Benyoussef, A. Magnetic Properties of $MnCr_2O_4$ Nanoparticle. *J. Magn. Magn. Mater.* **2010**, *322*, 301−304.
(15) El Moussaoui, H.; Mahfoud, T.; Ben Ali, M.; Mahhouti, Z.; Masrour, R.; Hamedoun, M.; Hlil, E. K.; Benyoussef, A. Experimental Studies of Neodymium Ferrites Doped with Three Different Transition Metals. *Mater. Lett.* **2016**, *171*, 142−145.
(16) El Moussaoui, H.; Mahfoud, T.; Habouti, S.; El Maalam, K.; Ben Ali, M.; Hamedoun, M.; Mounkachi, O.; Masrour, R.; Hlil, E. K.; Benyoussef, A. Synthesis and Magnetic Properties of Tin Spinel Ferrites Doped Manganese. *J. Magn. Magn. Mater.* **2016**, *405*, 181−186.
(17) Ben Ali, M.; El Maalam, K.; El Moussaoui, H.; Mounkachi, O.; Hamedoun, M.; Masrour, R.; Hlil, E. K.; Benyoussef, A. Effect of zinc concentration on the structural and magnetic properties of mixed Co-Zn ferrites nanoparticles synthesized by sol/gel method. *J. Magn. Magn. Mater.* **2016**, *398*, 20−25.
(18) Mameli, V.; Musinu, A.; Ardu, A.; Ennas, G.; Peddis, D.; Niznansky, D.; Sangregorio, C.; Innocenti, C.; Thanh, N. T. K.; Cannas, C. Studying the Effect of Zn-Substitution on the Magnetic and Hyperthermic Properties of Cobalt Ferrite Nanoparticles. *Nanoscale* **2016**, *8*, 10124−10137.
(19) Angotzi, M. S.; Mameli, V.; Cara, C.; Ardu, A.; Nizňanský, D.; Musinu, A. Oleate-Based Solvothermal Approach for Size Control of $M^{II}Fe^{III}_2O_4$ (M^{II} = Mn^{II}, Fe^{II}) Colloidal Nanoparticles. *J. Nanosci. Nanotechnol.* **2019**, *19*, 4954−4963.
(20) Hochepied, J. F.; Pileni, M. P. Magnetic properties of mixed cobalt-zinc ferrite nanoparticles. *J. Appl. Phys.* **2000**, *87*, 2472−2478.
(21) Calero-DdelC, V. L.; Rinaldi, C. Synthesis and Magnetic Characterization of Cobalt-Substituted Ferrite ($Co_xFe_{3-x}O_4$) Nanoparticles. *J. Magn. Magn. Mater.* **2007**, *314*, 60−67.
(22) Choi, H. N.; Hyun, S. W.; Shim, I.-B.; Kim, C. S. A Study of Co Substituted Mn-Ferrite, $Mn_{1-x}Co_xFe_2O_4$ (x=0.0,0.5,1.0). *IEEE Trans. Magn.* **2009**, *45*, 2554−2556.
(23) Kim, C. H.; Myung, Y.; Cho, Y. J.; Kim, H. S.; Park, S.-H.; Park, J.; Kim, J.-Y.; Kim, B. Electronic Structure of Vertically Aligned Mn-

Doped $CoFe_2O_4$ Nanowires and Their Application as Humidity Sensors and Photodetectors. *J. Phys. Chem. C* **2009**, *113*, 7085−7090.
(24) Ati, A. A.; Abdalsalam, A. H.; Hasan, A. S. Thermal, Microstructural and Magnetic Properties of Manganese Substitution Cobalt Ferrite Prepared via Co-Precipitation Method. *J. Mater. Sci.: Mater. Electron.* **2021**, *32*, 3019−3037.
(25) Yamada, S.; Shigesawa, R.; Latiff, H.; Kishimoto, M.; Kita, E.; Yanagihara, H. Magnetic Properties of Tetragonal Cobalt Manganese Ferrite Particles Prepared Using the Molten Salt Method. *IEEE Trans. Magn.* **2020**, *56*, 6702618.
(26) Awad, K. R.; Wahsh, M. M. S.; El-Wakeel, S. T.; Ochiabuto, K. I.; Othman, A. G. M.; El-Sherif, I. Y.; El-Sherif, I. Y. $Mn_{0.2}Co_{0.8}Fe_2O_4$ and Encapsulated $Mn_{0.2}Co_{0.8}Fe_2O_4/SiO_2$ Magnetic Nanoparticles for Efficient Pb2p Removal from Aqueous Solution. *Water Sci. Technol.* **2019**, *80*, 377−386.
(27) Ahsan, M. Z.; Khan, F. A.; Islam, M. A. Frequency and Temperature Dependent Intrinsic Electric Properties of Manganese Doped Cobalt Ferrite Nanoparticles. *Results Phys.* **2019**, *14*, 102484.
(28) Aslibeiki, B.; Kameli, P.; Salamati, H.; Concas, G.; Fernandez, M.; Salvador Fernandez, A.; Muscas, G.; Peddis, D. Co-Doped $MnFe_2O_4$ Nanoparticles: Magnetic Anisotropy and Interparticle Interactions. *Beilstein J. Nanotechnol.* **2019**, *10*, 856−865.
(29) Abdel Maksoud, M. I. A.; El-ghandour, A.; El-Sayyad, G. S.; Awed, A. S.; Ashour, A. H.; El-Batal, A. I.; Gobara, M.; Abdel-Khalek, E. K.; El-Okr, M. M. Incorporation of Mn^{2+} into Cobalt Ferrite via Sol−Gel Method: Insights on Induced Changes in the Structural, Thermal, Dielectric, and Magnetic Properties. *J. Sol-Gel Sci. Technol.* **2019**, *90*, 631−642.
(30) Aquino, V. R. R.; Vinícius-Araújo, M.; Shrivastava, N.; Sousa, M. H.; Coaquira, J. A. H.; Bakuzis, A. F. Role of the Fraction of Blocked Nanoparticles on the Hyperthermia Efficiency of Mn-Based Ferrites at Clinically Relevant Conditions. *J. Phys. Chem. C* **2019**, *123*, 27725−27734.
(31) Keswani, B. C.; Patil, S. I.; Kolekar, Y. D.; Ramana, C. V. Improved Magnetostrictive Properties of Cobalt Ferrite ($CoFe_2O_4$) by Mn and Dy Co-Substitution for Magneto-Mechanical Sensors. *J. Appl. Phys.* **2019**, *126*, 174503.
(32) Xiong, Y.; Yang, Y.; Feng, X.; DiSalvo, F. J.; Abruña, H. D. A Strategy for Increasing the Efficiency of the Oxygen Reduction Reaction in Mn-Doped Cobalt Ferrites. *J. Am. Chem. Soc.* **2019**, *141*, 4412−4421.
(33) Ahsan, M. Z.; Khan, F. A.; Islam, M. A. Frequency and Temperature Dependent Dielectric and Magnetic Properties of Manganese Doped Cobalt Ferrite Nanoparticles. *J. Electron. Mater.* **2019**, *48*, 7721−7729.
(34) Abdel Maksoud, M. I. A.; El-Sayyad, G. S.; Abd Elkodous, M.; Awed, A. S. Controllable Synthesis of $Co_{1-x}M_xFe_2O_4$ Nanoparticles (M = Zn, Cu, and Mn; x = 0.0 and 0.5) by Cost-Effective Sol−Gel Approach: Analysis of Structure, Elastic, Thermal, and Magnetic Properties. *J. Mater. Sci.: Mater. Electron.* **2020**, *31*, 9726−9741.
(35) Naik, A. B.; Naik, P. P.; Hasolkar, S. S.; Naik, D. Structural, magnetic and electrical properties along with antifungal activity & adsorption ability of cobalt doped manganese ferrite nanoparticles synthesized using combustion route. *Ceram. Int.* **2020**, *46*, 21046−21055.
(36) Jabbar, R.; Sabeeh, S. H.; Hameed, A. M. Structural, Dielectric and Magnetic Properties of Mn^{+2} Doped Cobalt Ferrite Nanoparticles. *J. Magn. Magn. Mater.* **2020**, *494*, 165726.
(37) Hou, Y. H.; Yan, X. T.; Huang, Y. L.; Zheng, S. H.; Hou, S. J.; Ouyang, Y. F. Structural, Electronic and Magnetic Properties of Manganese Substituted $CoFe_2O_4$: A First-Principles Study. *J. Magn. Magn. Mater.* **2020**, *495*, 165862.
(38) Dou, R.; Cheng, H.; Ma, J.; Komarneni, S. Manganese Doped Magnetic Cobalt Ferrite Nanoparticles for Dye Degradation via a Novel Heterogeneous Chemical Catalysis. *Mater. Chem. Phys.* **2020**, *240*, 122181.
(39) Mdlalose, W. B.; Dlamini, S.; Moyo, T.; Mokhosi, S. R.; Singh, M. Chitosan Coating by Mechanical Milling of $MnFe_2O_4$ and $Mn_{0.5}Co_{0.5}Fe_2O_4$: Effect of Milling. *J. Phys.: Conf. Ser.* **2019**, *1310*, 012016.
(40) Farheen, A.; Singh, R. Effect of Mn Substitution on Structure and Magnetic Properties of Cobalt Ferrite Nanoparticles. *Integr. Ferroelectr.* **2019**, *203*, 91−96.
(41) Nasrin, S.; Chowdhury, F.-U. -Z.; Hoque, S. M. Study of Hyperthermia Temperature of Manganese-Substituted Cobalt Nano Ferrites Prepared by Chemical Co-Precipitation Method for Biomedical Application. *J. Magn. Magn. Mater.* **2019**, *479*, 126−134.
(42) Bhame, S. D.; Joy, P. A. Enhanced Magnetostrictive Properties of Mn Substituted Cobalt Ferrite $Co_{1.2}Fe_{1.8}O_4$. *J. Appl. Phys.* **2006**, *99*, 073901.
(43) Qi, F.; Xu, B.; Chu, W. Heterogeneous Catalytic Ozonation of Phenacetin in Water Using Magnetic Spinel Ferrite as Catalyst: Comparison of Surface Property and Efficiency. *J. Mol. Catal. A: Chem.* **2015**, *396*, 164−173.
(44) Ramadoss, G.; Suriyaraj, S. P.; Sivaramakrishnan, R.; Pugazhendhi, A.; Rajendran, S. Mesoporous Ferromagnetic Manganese Ferrite Nanoparticles for Enhanced Visible Light Mineralization of Azoic Dye into Nontoxic By-Products. *Sci. Total Environ.* **2021**, *765*, 142707.
(45) Elmaci, G.; Frey, C. E.; Kurz, P.; Zümreoğlu-Karan, B. Water Oxidation Catalysis by Using Nano-Manganese Ferrite Supported 1D-(Tunnelled), 2D-(Layered) and 3D-(Spinel) Manganese Oxides. *J. Mater. Chem. A* **2016**, *4*, 8812−8821.
(46) Stolyarchuk, I. L.; Dolgikh, L. Y.; Vasilenko, I. V.; Pyatnitskii, Y. I.; Strizhak, P. E. Catalysis of Steam Reforming of Ethanol by Nanosized Manganese Ferrite for Hydrogen Production. *Theor. Exp. Chem.* **2012**, *48*, 129−134.
(47) Mameli, V.; Angotzi, M. S.; Cara, C.; Cannas, C. Liquid Phase Synthesis of Nanostructured Spinel Ferrites-A Review. *J. Nanosci. Nanotechnol.* **2019**, *19*, 4857−4887.
(48) Abdallah, H. M. I.; Moyo, T.; Msomi, J. Z. Mössbauer and Electrical Studies of $Mn_xCo_{1-x}Fe_2O_4$ Compounds Prepared via Glycothermal Route. *J. Supercond. Novel Magn.* **2011**, *24*, 669−673.
(49) Msomi, J. Z.; Abdallah, H. M. I.; Moyo, T.; Lančok, A. Structural and Magnetic Properties of $Mn_xCo_{1-x}Fe_2O_4$ Ferrite Nanoparticles. *J. Magn. Magn. Mater.* **2011**, *323*, 471−474.
(50) Abdallah, H. M. I.; Moyo, T.; Msomi, J. Z. The Effect of Annealing Temperature on the Magnetic Properties of $Mn_xCo_{1-x}Fe_2O_4$ Ferrites Nanoparticles. *J. Supercond. Novel Magn.* **2012**, *25*, 2625−2630.
(51) Köseoğlu, Y.; Alan, F.; Tan, M.; Yilgin, R.; Öztürk, M. Low Temperature Hydrothermal Synthesis and Characterization of Mn Doped Cobalt Ferrite Nanoparticles. *Ceram. Int.* **2012**, *38*, 3625−3634.
(52) Topkaya, R.; Akman, Ö.; Kazan, S.; Aktaş, B.; Durmus, Z.; Baykal, A. Surface Spin Disorder and Spin-Glass-like Behaviour in Manganese-Substituted Cobalt Ferrite Nanoparticles. *J. Nanopart. Res.* **2012**, *14*, 1156.
(53) Abdallah, H. M. I.; Moyo, T. The Influence of Annealing Temperature on the Magnetic Properties of $Mn_{0.5}Co_{0.5}Fe_2O_4$ Nanoferrites Synthesized via Mechanical Milling Method. *J. Supercond. Novel Magn.* **2013**, *26*, 1361−1367.
(54) Hamedoun, M.; Masrour, R.; Mounkachi, O.; El moussaoui, H.; Benyoussef, A.; Hlil, E. K. Physical Properties of $Co(Mn)Fe_2O_4$ Nanomaterials. *Phys. Scr.* **2013**, *88*, 015704.
(55) Fernandes, C.; Pereira, C.; Fernández-García, M. P.; Pereira, A. M.; Guedes, A.; Fernández-Pacheco, R.; Ibarra, A.; Ibarra, M. R.; Araújo, J. P.; Freire, C. Tailored Design of $Co_xMn_{1-x}Fe_2O_4$ Nanoferrites: A New Route for Dual Control of Size and Magnetic Properties. *J. Mater. Chem. C* **2014**, *2*, 5818−5828.
(56) Ahalya, K.; Suriyanarayanan, N.; Ranjithkumar, V. Effect of Cobalt Substitution on Structural and Magnetic Properties and Chromium Adsorption of Manganese Ferrite Nano Particles. *J. Magn. Magn. Mater.* **2014**, *372*, 208−213.
(57) Yadav, S. P.; Shinde, S. S.; Kadam, A. A.; Rajpure, K. Y. Structural, Morphological, Dielectrical, Magnetic and Impedance Properties of $Co_{1-x}Mn_xFe_2O_4$. *J. Alloys Compd.* **2013**, *555*, 330−334.
(58) Ranjith Kumar, E.; Jayaprakash, R.; Arunkumar, T.; Kumar, S. Effect of Reaction Time on Particle Size and Dielectric Properties of

https://doi.org/10.1021/acs.jpcc.1c06211
J. Phys. Chem. C 2021, 125, 20626−20638

Manganese Substituted $CoFe_2O_4$ Nanoparticles. *J. Phys. Chem. Solids* **2013**, *74*, 110−114.
(59) Salunkhe, A. B.; Khot, V. M.; Phadatare, M. R.; Thorat, N. D.; Joshi, R. S.; Yadav, H. M.; Pawar, S. H. Low Temperature Combustion Synthesis and Magnetostructural Properties of Co-Mn Nanoferrites. *J. Magn. Magn. Mater.* **2014**, *352*, 91−98.
(60) Atif, M.; Sato Turtelli, R.; Grössinger, R.; Siddique, M.; Nadeem, M. Effect of Mn Substitution on the Cation Distribution and Temperature Dependence of Magnetic Anisotropy Constant in $Co_{1-x}Mn_xFe_2O_4$ ($0.0 \leq x \leq 0.4$) Ferrites. *Ceram. Int.* **2014**, *40*, 471−478.
(61) Vlazan, P.; Miron, I.; Sfirloaga, P. Cobalt Ferrite Substituted with Mn: Synthesis Method, Characterization and Magnetic Properties. *Ceram. Int.* **2015**, *41*, 3760−3765.
(62) Tanna, A. R.; Sosa, K. M.; Joshi, H. H. Study of Superparamagnetic Nano Particles of $Mn_xCo_{1-x}Fe_2O_4$ Ferrite System Prepared by Co-Precipitation Technique. *Mater. Res. Express* **2017**, *4*, 115010.
(63) Song, Q.; Zhang, Z. J. Controlled Synthesis and Magnetic Properties of Bimagnetic Spinel Ferrite $CoFe_2O_4$ and $MnFe_2O_4$ Nanocrystals with Core-Shell Architecture. *J. Am. Chem. Soc.* **2012**, *134*, 10182−10190.
(64) Angotzi, M. S.; Mameli, V.; Musinu, A.; Nizňanský, D. ^{57}Fe Mössbauer Spectroscopy for the Study of Nanostructured Mixed Mn−Co Spinel Ferrites. *J. Nanosci. Nanotechnol.* **2019**, *19*, 5008−5013.
(65) Sanna Angotzi, M.; Mameli, V.; Cara, C.; Peddis, D.; Xin, H. L.; Sangregorio, C.; Mercuri, M. L.; Cannas, C. On the synthesis of bimagnetic manganese ferrite-based core-shell nanoparticles. *Nanoscale Adv.* **2021**, *3*, 1612−1623.
(66) Young, R. A.; Wiles, D. B. Profile Shape Functions in Rietveld Refinements. *J. Appl. Crystallogr.* **1982**, *15*, 430−438.
(67) Mondini, S.; Ferretti, A. M.; Puglisi, A.; Ponti, A. Pebbles and PebbleJuggler: Software for Accurate, Unbiased, and Fast Measurement and Analysis of Nanoparticle Morphology from Transmission Electron Microscopy (TEM) Micrographs. *Nanoscale* **2012**, *4*, 5356−5372.
(68) Van Rijssel, J.; Kuipers, B. W. M.; Erné, B. H. Non-Regularized Inversion Method from Light Scattering Applied to Ferrofluid Magnetization Curves for Magnetic Size Distribution Analysis. *J. Magn. Magn. Mater.* **2014**, *353*, 110−115.
(69) Bender, P.; Balceris, C.; Ludwig, F.; Posth, O.; Bogart, L. K.; Szczerba, W.; Castro, A.; Nilsson, L.; Costo, R.; Gavilán, H.; et al. Distribution Functions of Magnetic Nanoparticles Determined by a Numerical Inversion Method. *New J. Phys.* **2017**, *19*, 73012.
(70) Bender, P.; Bogart, L. K.; Posth, O.; Szczerba, W.; Rogers, S. E.; Castro, A.; Nilsson, L.; Zeng, L. J.; Sugunan, A.; Sommertune, J.; et al. Structural and Magnetic Properties of Multi-Core Nanoparticles Analysed Using a Generalised Numerical Inversion Method. *Sci. Rep.* **2017**, *7*, 45990.
(71) Morrish, A. H. *The Physical Principles of Magnetism*; Wiley, 1965.
(72) Boni, A.; Basini, A. M.; Capolupo, L.; Innocenti, C.; Corti, M.; Cobianchi, M.; Orsini, F.; Guerrini, A.; Sangregorio, C.; Lascialfari, A. Optimized PAMAM Coated Magnetic Nanoparticles for Simultaneous Hyperthermic Treatment and Contrast Enhanced MRI Diagnosis. *RSC Adv.* **2017**, *7*, 44104−44111.
(73) Kelly, P. E.; O'Grady, K.; Mayo, P. I.; Chantrell, R. W. Switching Mechanisms in Cobalt-Phosphorus Thin Films. *IEEE Trans. Magn.* **1989**, *25*, 3881−3883.
(74) Matsnev, M. E.; Rusakov, V. S. SpectrRelax: An Application for Mössbauer Spectra Modeling and Fitting. In *AIP Conference Proceedings*; 2012, pp 178−185.
(75) Shannon, R. D.; Prewitt, C. T. Revised Values of Effective Ionic Radii. *Acta Crystallogr., Sect. B: Struct. Crystallogr. Cryst. Chem.* **1970**, *26*, 1046−1048.
(76) Bhame, S. D.; Joy, P. A. Magnetic and Magnetostrictive Properties of Manganese Substituted Cobalt Ferrite. *J. Phys. D: Appl. Phys.* **2007**, *40*, 3263−3267.
(77) Walker, M.; Mayo, P. I.; O'Grady, K.; Charles, S. W.; Chantrell, R. W. The Magnetic Properties of Single-Domain Particles with Cubic Anisotropy. I. Hysteresis Loops. *J. Phys.: Condens. Matter* **1993**, *5*, 2779−2792.
(78) Manikandan, A.; Durka, M.; Antony, S. A. Role of Mn^{2+} Doping on Structural, Morphological, and Opto-Magnetic Properties of Spinel $Mn_xCo_{1-x}Fe_2O_4$ (x = 0.0, 0.1, 0.2, 0.3, 0.4, and 0.5) Nanocatalysts. *J. Supercond. Novel Magn.* **2015**, *28*, 2047−2058.
(79) Adeela, N.; Maaz, K.; Khan, U.; Karim, S.; Nisar, A.; Ahmad, M.; Ali, G.; Han, X. F.; Duan, J. L.; Liu, J. Influence of Manganese Substitution on Structural and Magnetic Properties of $CoFe_2O_4$ Nanoparticles. *J. Alloys Compd.* **2015**, *639*, 533−540.
(80) Henkel, O. Remanenzverhalten Und Wechselwirkungen in Hartmagnetischen Teilchenkollektiven. *Phys. Status Solidi* **1964**, *7*, 919−929.
(81) De Toro, J. A.; Vasilakaki, M.; Lee, S. S.; Andersson, M. S.; Normile, P. S.; Yaacoub, N.; Murray, P.; Sánchez, E. H.; Muñiz, P.; Peddis, D.; et al. Remanence Plots as a Probe of Spin Disorder in Magnetic Nanoparticles. *Chem. Mater.* **2017**, *29*, 8258−8268.
(82) Muscas, G.; Cobianchi, M.; Lascialfari, A.; Cannas, C.; Musinu, A.; Omelyanchik, A.; Rodionova, V.; Fiorani, D.; Mameli, V.; Peddis, D. Magnetic Interactions Versus Magnetic Anisotropy in Spinel Ferrite Nanoparticles. *IEEE Magn. Lett.* **2019**, *10*, 6110305.
(83) Laureti, S.; Varvaro, G.; Testa, A. M.; Fiorani, D.; Agostinelli, E.; Piccaluga, G.; Musinu, A.; Ardu, A.; Peddis, D. Magnetic Interactions in Silica Coated Nanoporous Assemblies of $CoFe_2O_4$ Nanoparticles with Cubic Magnetic Anisotropy. *Nanotechnology* **2010**, *21*, 315701.
(84) Kaman, O.; Kubániová, D.; Knížek, K.; Kubíčková, L.; Klementová, M.; Kohout, J.; Jirák, Z. Structure and Magnetic State of Hydrothermally Prepared Mn-Zn Ferrite Nanoparticles. *J. Alloys Compd.* **2021**, *888*, 161471.
(85) Zákutná, D.; Nižňanský, D.; Barnsley, L. C.; Babcock, E.; Salhi, Z.; Feoktystov, A.; Honecker, D.; Disch, S. Field Dependence of Magnetic Disorder in Nanoparticles. *Phys. Rev. X* **2020**, *10*, 031019.
(86) Gütlich, P.; Bill, E.; Trautwein, A. X. *Mössbauer Spectroscopy and Transition Metal Chemistry: Fundamentals and Applications*; Springer Berlin Heidelberg, 2010.
(87) Kubickova, S.; Niznansky, D.; Morales Herrero, M. P.; Salas, G.; Vejpravova, J. Structural Disorder versus Spin Canting in Monodisperse Maghemite Nanocrystals. *Appl. Phys. Lett.* **2014**, *104*, 223105.
(88) Smit, J.; Wijn, H. P. J. Ferrites. *Philips' Technical Library*; Scientific Research Publishing, 1959.
(89) Vamvakidis, K.; Katsikini, M.; Sakellari, D.; Paloura, E. C.; Kalogirou, O.; Dendrinou-Samara, C. Reducing the Inversion Degree of $MnFe_2O_4$ Nanoparticles through Synthesis to Enhance Magnetization: Evaluation of Their (1)H NMR Relaxation and Heating Efficiency. *Dalton Trans.* **2014**, *43*, 12754−12765.
(90) Fantechi, E.; Campo, G.; Carta, D.; Corrias, A.; de Julián Fernández, C.; Gatteschi, D.; Innocenti, C.; Pineider, F.; Rugi, F.; Sangregorio, C. Exploring the Effect of Co Doping in Fine Maghemite Nanoparticles. *J. Phys. Chem. C* **2012**, *116*, 8261−8270.
(91) Carta, D.; Casula, M. F.; Falqui, A.; Loche, D.; Mountjoy, G.; Sangregorio, C.; Corrias, A. A Structural and Magnetic Investigation of the Inversion Degree in Ferrite Nanocrystals MFe_2O_4 (M = Mn, Co, Ni). *J. Phys. Chem. C* **2009**, *113*, 8606−8615.
(92) Blanco-Gutiérrez, V.; Gallastegui, J. A.; Bonville, P.; Torralvo-Fernández, M. J.; Sáez-Puche, R. MFe_2O_4 (M: Co^{2+}, Ni^{2+}) Nanoparticles: Mössbauer and X-Ray Absorption Spectroscopies Studies and High-Temperature Superparamagnetic Behavior. *J. Phys. Chem. C* **2012**, *116*, 24331−24339.

https://doi.org/10.1021/acs.jpcc.1c06211
J. Phys. Chem. C 2021, 125, 20626−20638